ARTICLE IN PRESS

INTERNATIONAL JOURNAL OF HYDROGEN ENERGY XXX (XXXX) XXX

Available online at www.sciencedirect.com

ScienceDirect

journal homepage: www.elsevier.com/locate/he

Vapor/gas separation through carbon molecular sieve membranes: Experimental and theoretical investigation

Serena Poto [a], *Joost G.H. Endepoel* [a], *Margot Anabell Llosa-Tanco* [b], *David Alfredo Pacheco-Tanaka* [b], *Fausto Gallucci* [a,c,*], *M. Fernanda Neira d'Angelo* [a,**]

[a] *Sustainable Process Engineering, Chemical Engineering and Chemistry, Eindhoven University of Technology, De Rondom 70, 5612, Eindhoven, the Netherlands*

[b] *TECNALIA, Basque Research and Technology Alliance (BRTA), Mikeletegi Pasealekua 2, 20009, Donostia-San Sebastián, Spain*

[c] *Eindhoven Institute for Renewable Energy Systems (EIRES), Eindhoven University of Technology, PO Box 513, Eindhoven, 5600, the Netherlands*

HIGHLIGHTS

- Several boehmite-phenolic resin composite carbon molecular sieve membranes were developed.
- The hydrophilic boehmite nanosheets were used to increase the adsorption of water.
- Water permeability shows an optimum with the initial boehmite content around 0.8 wt. %.
- CMSM are promising material for the water separation from gaseous mixtures at relatively high temperatures.

ARTICLE INFO

Article history:
Received 29 June 2021
Received in revised form
15 October 2021
Accepted 21 October 2021
Available online xxx

Keywords:
Carbon membranes
Water separation
Hydrophilicity
Capillary condensation
CO_2 hydrogenation
Alumina-CMSM

ABSTRACT

The separation of H_2O vapor from (hydrogen-rich) gaseous streams is a topic of increasing interest in the context of CO_2 valorisation, where the *in situ* water removal increases product yield and catalyst stability. In this work, composite alumina carbon molecular sieve membranes (Al-CMSM) were prepared from phenolic resin solutions loaded with hydrophilic boehmite (γ-AlO(OH)) nanosheets (0.4–1.4 wt. % in solution) which partially transform to γ-Al_2O_3 nanosheets upon thermal decomposition of the resin, improving the hydrophilicity and thus the adsorption-diffusion contribution of the H_2O permeation. The γ-Al_2O_3 nanosheets showed no influence on the pore size distribution of the membranes in the range of micropores, but they increased the membrane hydrophilicity. In addition, the use of boehmite in the resin solution causes an increase in the viscosity and thus an increase in the carbon layers thickness deposited on the porous α-Al_2O_3 support (from 1 to 3.3 μm). Furthermore, the alumina sheets introduce defects in the carbon matrix, increasing the tortuosity of the active layer, as concluded via phenomenological modelling and parametric fitting of the experimental results. As a consequence, the water permeability exhibits a maximum ($1.3 \cdot 10^{-6}$ mol·s^{-1} Pa^{-1} m^{-1} at 150 °C) with boehmite/alumina content of ca. 0.8 wt. %, as the combined effects of increasing hydrophilicity (which favour

* *Corresponding author*. Sustainable Process Engineering, Chemical Engineering and Chemistry, Eindhoven University of Technology, De Rondom 70, 5612, Eindhoven, the Netherlands.

** *Corresponding author*.

E-mail addresses: F.Gallucci@tue.nl (F. Gallucci), M.F.Neira.dAngelo@tue.nl (M.F. Neira d'Angelo).

https://doi.org/10.1016/j.ijhydene.2021.10.155

0360-3199/© 2021 The Author(s). Published by Elsevier Ltd on behalf of Hydrogen Energy Publications LLC. This is an open access article under the CC BY license (http://creativecommons.org/licenses/by/4.0/).

Please cite this article as: Poto S et al., Vapor/gas separation through carbon molecular sieve membranes: Experimental and theoretical investigation, International Journal of Hydrogen Energy, https://doi.org/10.1016/j.ijhydene.2021.10.155

H_2O permeability) and increasing thickness and tortuosity (which hamper permeability) upon increasing boehmite loading. Similarly, the H_2O/gas perm-selectivity is optimum at 1.2 wt. % boehmite loading. We further investigated the H_2O permeation mechanism by modelling the mono- and multi-layer adsorption and capillary condensation of water in microporous media, which result as the main transport mechanisms in the explored conditions.
© 2021 The Author(s). Published by Elsevier Ltd on behalf of Hydrogen Energy Publications LLC. This is an open access article under the CC BY license (http://creativecommons.org/licenses/by/4.0/).

Nomenclature

Symbol, Definition, Units

κ_i	Permeability of component i, $mol\ m^{-1}s^{-1}Pa^{-1}$
$\wp_i$	Permeance of component i, $mol\ m^{-2}s^{-1}Pa^{-1}$
$S_{H_2O/i}$	Ideal perm-selectivity of H_2O towards component i
$SF_{H_2O/i}$	Separation factor of water towards component i
$W_{H_2O,\ perm.}$	Weight of water collected from the permeate, g
$M_{w,i}$	Molecular weight of component i, g/mol
Δt	Time span of the permeation experiment, s
ΔP_i	Gradient of partial pressure of component i across, Pa, the membrane
A_m	Membrane area, m^2
l	Thickness of the carbon layer, m
y_i	Molar fraction of component i
P_i	Partial pressure of component i, Pa
Φ_i	Volumetric flow of component i, mL/min
V_m	Standard molar volume of a gas, mL/mol
ΔP	Gradient of total pressure across the membrane, Pa
υ	Molar volume of water, mL/mol
σ	Water surface tension, N/m^2
θ	Contact angle, deg
r_p	Pore radius, m
P_0 or P_t	Capillary condensation pressure of water, Pa
P_s	Water saturation pressure on planar surface, Pa
A_p	Cross sectional area of the porous material, m^2
C_R	Coefficient of resistance,
$F_{c,eff}$	Effective capillary condensate flow,
F_g	Flow rate due to Knudsen flow, mol/s
F_s	Flow rate due to surface flow, mol/s
F_t	Total flow through the membrane, mol/s
G_1	Geometric constant of the membrane,
K_d	Pore structure constant
$P_{c,eff}$	Effective capillary pressure, Pa
P_c	Capillary suction pressure, Pa
P_m	Averaged gas pressure, Pa
PSD	Pore size distribution
$F_{j=1:6}$	Flow rate of flow type 1, 2, 3, 4, 5 and 6, mol/s
Q_c	Capillary condensate permeance, $mol\ m^{-2}s^{-1}Pa^{-1}$
Q_g	Knudsen flow gas permeance, $mol\ m^{-2}s^{-1}Pa^{-1}$
Q'_g	Knudsen flow gas permeance including pore blockage, $mol\ m^{-2}s^{-1}Pa^{-1}$
R	Ideal gas constant, $J\ mol^{-1}K^{-1}$
r_e	Effective pore radius, m
S_t	Specific surface areas of porous material, m^2/kg
η	Viscosity of water, $Pa{\cdot}s$
T	Temperature, K
t	Thickness of water adsorbed layer, m
x	Amount of adsorbed material, mol/kg

Subscripts

perm	or 2 Permeate
ret	or 1 Retentate

Introduction

In strive for sustainability, the use of membrane (reactor) technologies have proofed very attractive to increase resource and energy efficiency of various chemical processes [1–7]. In particular, they have gained increasing attention in recent years for the much-needed valorisation of CO_2, a greenhouse gas which is often considered as an expensive waste stream as well as the main responsible of global warming [8–11]. Most of the CO_2 valorisation routes proceed via hydrogenation reactions (e.g., CO_2 hydrogenation to methanol, ethanol, DME, CO, CH_4 etc.), where the large amount of water produced leads to thermodynamic limitations and, sometimes, to catalyst deactivation [12–14].

Several studies have already demonstrated, mainly from a theoretical perspective, that the use of hydrophilic membranes to promote the selective removal of H_2O has remarkable effects on the CO_2 conversion [15–24]. The selection of the membrane material is crucial, especially in terms of stability in hot humid environment [17]. For this reason, polymeric membranes are not suitable, since they cannot work at very high temperatures, and undergo plasticization and swelling phenomena. Porous inorganic membranes, on the other hand, have been extensively studied for pervaporation [25–30]. Ceramic membranes, in particular zeolites, have been mostly proposed for the in-situ removal of H_2O in different reactive systems [15–21,31,32]. Despites their excellent properties in terms of vapor permeability, mainly deriving from their strong hydrophilicity, zeolite membranes suffer from: 1)

Please cite this article as: Poto S et al., Vapor/gas separation through carbon molecular sieve membranes: Experimental and theoretical investigation, International Journal of Hydrogen Energy, https://doi.org/10.1016/j.ijhydene.2021.10.155

poor reproducibility, due to the complexity of the synthesis procedure [33,34] and 2) poor long-term stability when in contact with large volume of hot water due to dealumination [34,35]. Alternatively, carbon molecular sieve membranes (CMSM) offer superior thermo-chemical stability in humid and corrosive environments, as well as an excellent balance between gas permeance and perm-selectivity, especially with respect to polymeric membranes [36–38]. Thus, CMSM are a potentially attractive candidate to selectively separate H_2O from other gases in the temperature conditions of the CO_2 hydrogenation processes (i.e., 200–400 °C) [39,40].

Carbon-based membranes have emerged as promising material for gas separation processes, with a wide application spectrum, owing to the possibility to tailor the properties of the carbon active layer and thus the governing permeation mechanism to the desired separation. Most of these applications include the separation of mixtures of (dry) gases such as CO_2, N_2, CH_4, H_2 or mixtures of alkane/alkene at relatively low temperature (i.e., 20–80 °C) [38,41–51]. Only very recently they have been demonstrated for water vapor permeation, at temperatures above 150 °C [52]. Carbon membranes derive from the pyrolysis of a thermoset polymeric precursor in inert conditions or vacuum, typically deposited on the surface of a porous ceramic support (e.g., α-Al_2O_3). Depending on the conditions of the carbonization step (e.g., inert atmosphere, temperature, time and heating rate) and on the physicochemical properties of the precursor, their porous structure and degree of hydrophilicity/hydrophobicity can be tuned according to the desired application and its perm-selectivity requirements. Forster et al. [52] have recently reported that an increase in the carbonization temperature causes, on average, a shrinkage of the pore size and, at the same time, a decrease in the affinity to water. Indeed, when the temperature of carbonization is increased above 550–650 °C, most of the oxygen-based groups are removed. Upon decomposition of the polymeric precursor, the imperfections in the microcrystalline regions give rise to a porous structure which typically includes ultra-micropores (i.e., $d_p \leq 0.6$) and micropores (i.e., $0.6 \leq d_p \leq 2$) [53,54]. These are the main responsible for the separation mechanism via molecular sieving (i.e., based on size exclusion) and adsorption diffusion (i.e., based on physicochemical differential interactions between diffusing species and the membrane surface), respectively. Besides the pore structure and surface properties of the membrane, the operating temperature is a well-known parameter that determines the governing permeation mechanism. At higher temperatures, corresponding to higher molecular energy level, the collisions of the molecules with the pore walls are more frequent, slowing down the permeation process. This phenomenon is known as Knudsen diffusion [55]. Therefore, higher temperatures hinder the adsorption phenomena, and the transport mechanism inevitably turns into the molecular sieving or Knudsen diffusion [54,56]. For each diffusing gas, a specific temperature exists at which the adsorption-diffusion is not relevant anymore. Llosa et al. [44] reported that for temperatures above 180 °C and 80 °C, the adsorption-diffusion mechanism for CO_2 and CH_4, respectively, is negligible. At lower temperatures, on the other hand, when the adsorption-diffusion mechanism is dominant, the diffusing species could reduce the effective pore size of the membranes, hindering the permeation of the non-diffusing species. Therefore, at low temperatures, higher perm-selectivity values can be achieved.

While most of the literature on CMSM deals with (low temperature) gas separation processes, which are usually described as a combination of molecular sieving and/or adsorption-diffusion, very limited attention has been paid to the separation of mixtures containing condensable species like H_2O. In these cases, an additional transport mechanism via viscous flow of capillary condensate [57–59] should be contemplated. Indeed, for wetting systems (e.g., H_2O on a hydrophilic solid surface) the vapor pressure in a capillary is lower than that on a planar surface, as described by the Kelvin's equation [60]. Thus, water can condense in the micropores of the carbon membranes with sufficient hydrophilicity. The viscous flow of capillary condensate is usually slower than the multi- and mono-layer adsorption-diffusion [57], explaining the observed maxima in permeability vs. surface hydrophilicity reported by Forster et al. [52]. In other words, strengthening surface interactions (e.g. by decreasing temperature or tunning surface hydrophilicity/hydrophobicity) does not always render an increase in permeance. Whereas the existence of capillary condensation may be considered as a nuisance (i.e. lower permeability), or even complexing factor that obscures the interpretation of experimental data, it can surely be used for the rational design of a selective membrane if properly understood. When looking at the case of water separation, a hydrophilic carbon membrane is an obvious choice given their well-established affinity to H_2O [42,50]. Water is known to adsorb on the pores already at ambient conditions, reducing the active pore size of the membranes [62] and thereby increasing the separation factors between water and other gases. Even more, when capillary condensation occurs, water could partially or totally block the pores of the membranes, further supressing the permeation of the other gases. In processes involving CO_2 hydrogenation, where the focus is the selective separation of H_2O from reactants and products such as H_2, CO_2 and CO, this is for sure an enormous advantage.

In practical terms, the hydrophilicity of the carbon membrane can be tuned not only by selecting the proper polymer precursor and/or the conditions of the carbonization step [52]. Besides, the incorporation of additives like silica [63] or boehmite [64] in the carbon matrix have also proved to affect the gas permeability, due to an alteration of the pore distribution. However, the effect of those fillers on the membrane hydrophilicity has not been investigated yet. In this work, we study the effect of the concentration of boehmite nanosheets into the CMSM on the hydrophilicity of the membrane and its effect on water vapor permeation. For that purpose, we incorporate low-cost boehmite nanosheets in phenolic resin-based carbon membranes [64–66] for the separation of H_2O vapor from H_2, CO_2 CO, N_2 and CH_4 at 150–250 °C and 2–5 bar. The effect of boehmite loading is studied by correlating the membrane properties (assessed by gravimetric studies, morphological analysis such as XRD and XPS, pore size measurement, and cross section analysis via scanning electron microscopy) to performance data (i.e., permeabilities and separation factors). To gain a deeper understanding of the properties-performance correlations, the performance of these membranes is modelled using a phenomenological

Please cite this article as: Poto S et al., Vapor/gas separation through carbon molecular sieve membranes: Experimental and theoretical investigation, International Journal of Hydrogen Energy, https://doi.org/10.1016/j.ijhydene.2021.10.155

model describing the mono- and multi-layer adsorption and capillary condensation of water in microporous media (i.e., transport mechanisms involved in the permeation of pure H_2O-vapor in microporous media). Thus, the insights of this work are key for the rational design of selective CMSM membranes for water vapor separation.

Experimental

Synthesis of Al-CMSMs

The tubular Al-CMSMs were prepared by the one-dip dry carbonization step method, [64–66]. The supports are tubular asymmetric α-Al_2O_3 tubes (ID: 7 mm, OD: 10 mm), with a 100 nm average pore size, provided by Inopor®. The porous α-Al_2O_3 was attached to the dense Al_2O_3 by using a glass sealant at 1150 °C, leaving an effective length for the deposition of the carbon layer of about 10 cm. One end was closed with the glass seal, while the other end was connected to a standard Swagelok component to allow the flow of the permeate. The supports were dip-coated using a vacuum pump in a solution containing: 13% of Novolac resin, 0.6% of ethylenediamine, 2.4% of formaldehyde, a variable amount of 10% aqueous dispersion of boehmite nanosheets with a particle size of 8–20 nm (*Alumisol* provided by Kawaken fine Chemicals) [64], in order to obtain a boehmite content from 0.4 to 1.4%, and *N*-methyl-2-pyrrolidone (NMP) as solvent. Table 1 reports the boehmite content in the dipping solutions used for the preparation of the Al-CMSMs. The membranes were dried at 90 °C overnight under continuous rotation to guarantee a uniform and defect-free layer of the membrane precursor. Thereafter, the membranes were carbonized at 500 °C in inert atmosphere (i.e., 200 mL·min^{-1} of N_2). The remaining precursor solutions containing 0.8, 1.0 and 1.4 wt. % of boehmite nanosheets were used to prepare unsupported films for XRD and XPS analysis. The solution was placed in a Teflon dish, dried at 90 °C and carbonized following the same procedure described for the supported CMSM.

Permeation experiments

The permeation experiments were carried out in a dedicated setup whose layout is sketched in Fig. 1. The setup is characterized by three main modules: I) the feed module, II) the permeation module and III) the retentate/permeate analysis module. Mass flow controllers from Brook Instruments were used to feed the desired flow rate of H_2, CO_2, CO, CH_4 and N_2 (mL·min^{-1}). Demineralized water was fed with a Controlled Evaporator Mixer (C.E.M.) from Bronkhorst, which requires a minimum flow of N_2 (≥150 mL·min^{-1}) to allow the water to reach the reactor. To avoid steam condensation, tracing was installed in all the lines and set at a temperature of 200 °C. The permeation module consists of a stainless-steel vessel where the membrane is connected from the top flange. The vessel is placed in an electrical oven to keep isothermal conditions, controlling the temperature on the outer surface of the membrane. The pressure in the permeate side (i.e., inner tube of the membrane) was kept at 1 bar, while the pressure in the retentate side (i.e., outside of the membrane) is controlled with a back-pressure regulator from Bronkhorst. The analysis module consists of two condensers, a film flow meter (Horiba Stec) and a micro-GC (Agilent Technologies). The two condensers use a synthetic coolant supplied by the Lauda electric unit, to condense and collect liquid water from the retentate and the permeate. Thereafter, the gas flow rate from the permeate line was measured with the film flow meter and then injected to the micro-GC for the analysis of the composition.

Two types of permeation experiments were conducted for: a) pure gas or vapor permeation and b) binary vapor/gas mixture permeation tests. The pure gas/vapor permeation tests were performed at a temperature of 150–240 °C, a pressure gradient across the membrane of 3 bar and a total feed flow of 1 L·min^{-1}. The membrane was first exposed to a flux of water – containing 7.5 vol% of N_2 – for 40 min to ensure steady state operation. The N_2 permeated flow was measured and the water was collected and weighted from both the retentate and the permeate. The value of the N_2 flow was used to correct the partial pressures for a more accurate calculation of the water permeance. Afterward, a pure gas flow (H_2, CO_2, CO, CH_4 or N_2) was fed to the membrane section for the pure gas permeation measurement. A vapor permeation test was repeated prior to each gas permeation test, to ensure the same humidity condition of the membrane, which is a parameter that strongly affects the permeation of the gases [67]. These experiments were performed to gain insight into the effect of the alumina nanosheets on the permeation performance of the membranes. Thereafter, the membrane which showed the best performance (i.e., a trade-off of water permeance and water/gas selectivity) was selected for a deeper investigation. In particular, the binary vapor/gas mixture permeation tests were carried out to investigate the effect of the interaction between water and each gas on the water/gas selectivity. These experiments were performed by feeding a mixture of water vapor, N_2 and another gas (H_2, CO_2 and CO) with a concentration of 25–75 vol% of either H_2, CO_2 or CO, a total feed flow of 1 L·min^{-1}, a temperature of 150–240 °C and a pressure gradient of 3 bar. Lastly, the effect of the pressure gradient across the membrane was investigated at a temperature of 150 °C, with pure gas/vapor permeation tests. The water permeance ($\wp_{H_2O}$) and permeability (κ_{H_2O}) were determined according to Eq. (1) and Eq. (2), respectively.

$$\wp_{H_2O} = \frac{W_{H_2O,permeated} \cdot M_{w,H_2O}^{-1}}{\Delta t \cdot \Delta P_{H_2O} \cdot A_m} \quad (1)$$

$$\kappa_{H_2O} = \wp_{H_2O} \cdot l \quad (2)$$

Where $w_{H_2O,\ permeated}$ is the weight of the water collected from the permeate, M_{w,H_2O} is its molecular weight, Δt indicates the

Table 1 – Boehmite content in the dipping solutions used to prepare the Al-CMSMs.

Membrane ID	Boehmite (wt. %)
CM04	0.4
CM06	0.6
CM08	0.8
CM10	1.0
CM12	1.2
CM14	1.4

Please cite this article as: Poto S et al., Vapor/gas separation through carbon molecular sieve membranes: Experimental and theoretical investigation, International Journal of Hydrogen Energy, https://doi.org/10.1016/j.ijhydene.2021.10.155

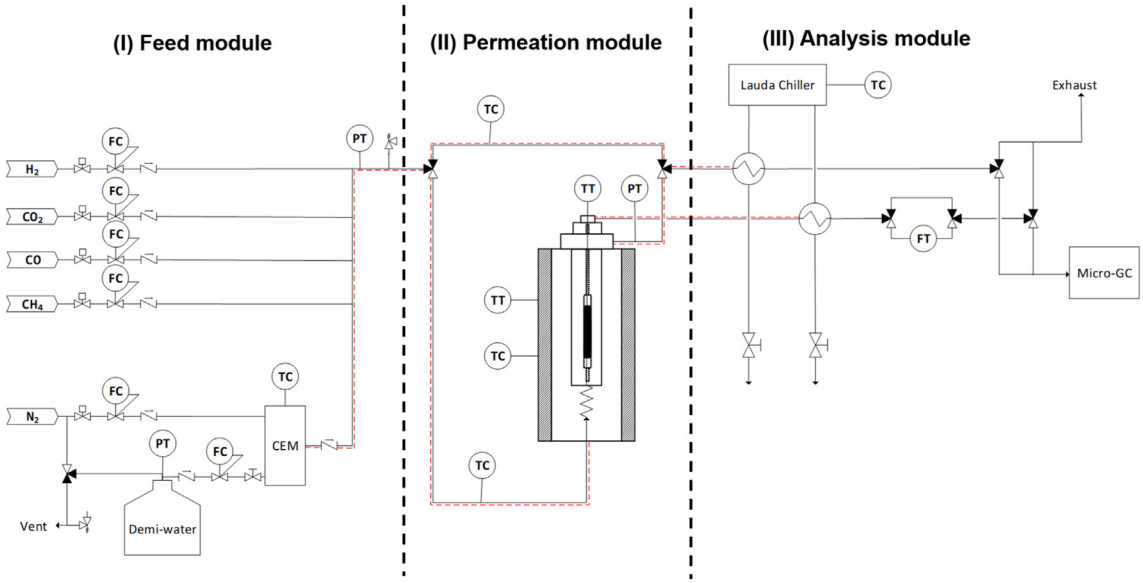

Fig. 1 – Layout of the setup designed for the vapor-gas permeation experiments. The setup is made up of three modules: (I) the feed module; (II) the permeation module and (III) the analysis module. TC, FC and PC represent the temperature, flow and pressure controller. Similarly, TT, FT and PT represent the temperature, flow and pressure transmitters.

time span of the permeation experiment, A_m and l are the membrane area and thickness, respectively. The $\wp_{H_2O}$ accounts for the presence of N_2 in the feed through the gradient of H_2O partial pressure across the membrane (ΔP_{H_2O}), defined according to Eq. (3).

$$\Delta P_{H_2O} = y_{H_2O,ret.} \cdot P_{ret.} - y_{H_2O,perm.} \cdot P_{perm.} \tag{3}$$

The gas permeance ($\wp_i$) was determined according to Eq. (4), with $\Phi_{i,perm}$ the volumetric flow rate of the permeated gas, V_m the standard molar volume of a gas and ΔP the gradient of total pressure across the membrane.

$$\wp_i = \frac{\Phi_{i,perm} \cdot V_m^{-1}}{\Delta P \cdot A_m} \tag{4}$$

The ideal H_2O/gas perm-selectivity ($S_{H_2O/i}$) and the H_2O/gas separation factors ($SF_{H_2O/i}$) were determined according to Eqs. (5) and (6), respectively.

$$S_{H_2O/i} = \frac{\wp_{H_2O}}{\wp_i} \tag{5}$$

$$SF_{H_2O/i} = \frac{[P_{H_2O}/P_i]_{permeate}}{[P_{H_2O}/P_i]_{retentate}} \tag{6}$$

Where the partial pressure of water (P_{H_2O}) and of the gas species (P_i) in the retentate/permeate, define the degree of separation.

Permporometry experiments

The pore size distribution of the membranes was measured via the permporometry technique, developed by Tsuru et al. [68]. The basic principle of this technique is the capillary condensation of a vapor and the corresponding pore blocking effect on the permeation of a non-condensable gas. This method has the advantage of being able to measure only the pores which are active for the permeation, discarding the dead-end pores. Furthermore, this method does not require the preparation of unsupported carbon films, the pore size distribution could be measured directly on the tubular carbon membranes, leading to a more realistic measurement. The experiments were carried out in a second permeation apparatus, where liquid water was injected via a syringe pump and vaporized in a heating coil; N_2 was used as a carrier gas. The vapor pressure of the stream was controlled by changing the N_2 flow rate. The N_2 permeated flow was measured after removing the water with a cold trap. The experiment was carried out at 70 °C and a ΔP across the membrane of 1 bar. Prior to each experiment, the membrane was dried at 150 °C under N_2 flow, until the N_2 permeance reached a stable value (i.e., corresponding to the membrane dry condition). The different values of water vapor pressure (P_0/P_s) imposed are directly related to the pore radius (r_p), through the Kelvin's equation (Eq. (7)).

$$RTln\left(\frac{P_0}{P_s}\right) = 2\upsilon\frac{\sigma\cos(\theta)}{r_p} \tag{7}$$

Where υ, σ and θ are the molar volume, surface tension and contact angle, respectively. The contact angle was assumed to be 0°, which is a typical assumption for the permporometry experiments [68]. When the vapor pressure of water was stepwise increased, a lower N_2 permeance was measured and the pore size distribution was derived.

Scanning electron microscopy (SEM)

A FEI Quanta scanning electron microscope was used to acquire images of the cross section of the CMSMs, to derive the thickness of the carbon layer. EDX was used to analyze the surface composition of the membranes qualitatively and to assess the uniform distribution of the Al_2O_3.

Please cite this article as: Poto S et al., Vapor/gas separation through carbon molecular sieve membranes: Experimental and theoretical investigation, International Journal of Hydrogen Energy, https://doi.org/10.1016/j.ijhydene.2021.10.155

X-ray diffraction (XRD) and X-Ray photoelectron spectroscopy (XPS) measurements

X-ray diffraction (XRD) analysis in the 2θ range 10–120° was performed on the carbon membrane films samples with a MiniFlex 600 machine (*Rigaku*) operating with a Ni β-filtered Cu-Kα radiant at 40 kV and 30 mA and a scan step of 0.05°/min. The diffraction peaks were identified according to the JCPDS database of reference compounds. XPS measurements were performed using a Kratos AXIS Ultra spectrometer, equipped with a monochromatic X-ray source, and a delay-line detector (DLD). Spectra were obtained using an aluminum anode (Al Kα = 1486.6eV) operating at 150 W. For both the XRD and XPS analyses, the carbon membrane films corresponding to the c-CMSM CM08, CM10 and CM14 were crushed to obtain a fine powder.

Gravimetric analysis

To assess the effect of the alumina content on the hydrophilicity of the CMSMs, the amount of water adsorbed by the membranes was measured via a gravimetric method. The carbon layer was scratched out from the tubular supported membrane and placed in a glass vial which was then kept in a climate chamber at a relative humidity of 99% at room temperature. The weight of the sample was recorded until saturation.

Theory of water transport through the CMSM

The transport of condensable vapors through porous media is a complex phenomenon involving capillary condensate flow, mono- and multi-layer adsorption, simultaneously. Many efforts have been made in the past years to theoretically describe the combination of these mechanisms [57,58,69,70]. In this work, the *six flows model,* developed by K. H. Lee and S. T. Hwang [58] was implemented to describe the water vapor permeation trough the carbon membranes. The objective here was to qualitatively understand which transport mechanism is predominant within the process conditions of this study and to find a correlation with the γ-Al_2O_3 content.

Model description

The permeation through porous media can be categorized in three different types: gas flow, surface flow and capillary condensate flow. The detailed equations describing these mechanisms are reported in the Supplementary Information (SI). Understanding the relative contribution of these flow types allows insight on the overall transport mechanisms of water vapor trough the membrane. The combination of those flows, together with the blocking effect exerted by the adsorbed layer, give rise to six types of flows (Fig. 2), which can be determined according to: 1) the relative pressure of the permeate (P_2) and the retentate (P_1), with respect to the capillary condensation pressure (P_0) (P_2/P_0 and P_1/P_0, respectively), and 2) the relative thickness of the adsorbed layer of water at the permeate (t_2) and retentate (t_1) with respect to the pore radius (r_p) (t_2/r_p and t_1/r_p, respectively). A detailed description of the phenomena is given below:

- F_1: Combination of Knudsen molecular flow (gas flow) and surface flow in the adsorbed phase.
- F_2: Capillary condensation occurs at the upstream end of the pore, but not at the downstream end. On the downstream side, gas and adsorbate flows take place.
- F_3: The entire pore is filled with a capillary condensate.
- F_4: The upstream end of the pore is filled with bulk condensate. Somewhere in the capillary (z) the meniscus is located. There is no curved interphase at the upstream side, therefore no suction force.
- F_5: The entire pore is filled with a capillary condensate. Capillary condensation occurs at the downstream side. The upstream end of the pore is filled with bulk condensate.
- F_6: The entire pore is filled with a capillary condensate and no meniscus is present in the pore.

The equations in Table 2 represent the mathematical expressions to compute the flow rate and the permeance according to each flow type. The physical properties for water vapor were obtained with empirical correlations as a function of temperature and pressure, as reported in SI. The pore size distribution of the carbon membrane was accounted for with a fitted Gaussian function and used to determine the total flow rate of the permeate trough the membrane as follows:

$$F_t = \int_0^\infty f(r) F_r dr \tag{8}$$

Model implementation

The six flows model was implemented in MATLAB R2019a. The pore size distribution, the membrane characteristics and the physical properties of water are given as input parameters. The boundary conditions (i.e., temperature and pressures) are defined as those of the permeation experiments. The flow mode is defined for each pore size (*r*) and Eq. (8) is

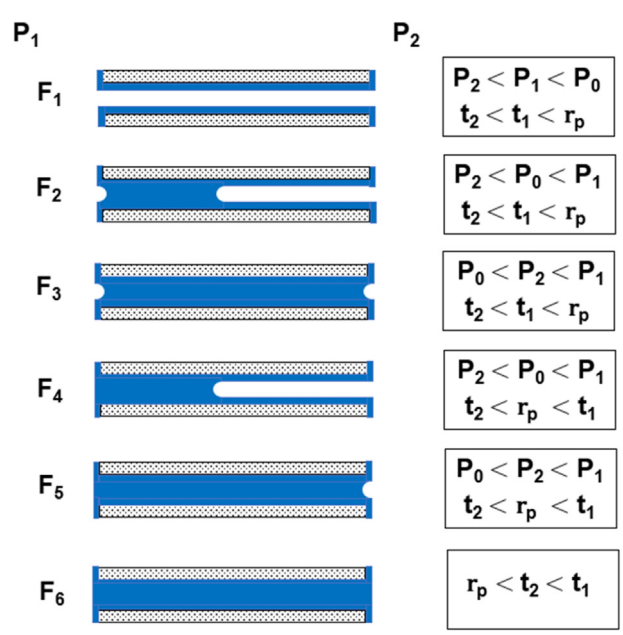

Fig. 2 – Six different flow modes of water permeation with their boundary conditions.

Please cite this article as: Poto S et al., Vapor/gas separation through carbon molecular sieve membranes: Experimental and theoretical investigation, International Journal of Hydrogen Energy, https://doi.org/10.1016/j.ijhydene.2021.10.155

Table 2 – Equations describing the flow rate of water through the pore according to each flow mode.

Flow mode	Equation
F_1	$F_1 = A_p(Q'_g + Q_s)\frac{\Delta P}{l}$
F_2	$F_2 = A_p(Q'_g + Q_s)\frac{P_0 - P_2}{l - z}$
F_3	$F_3 = \frac{A_p K_d}{\eta z}\frac{\rho RT}{M}\left[\frac{(r-t_1)^2}{r_p^2}ln\left(\frac{P_1}{P_0}\right) - \frac{(r-t_2)^2}{r_p^2}ln\left(\frac{P_2}{P_0}\right)\right]$
F_4	$F_4 = A_p(Q'_g + Q_s)\frac{P_0 - P_2}{l - z}$
F_5	$F_5 = \frac{A_p K_d}{\eta z}\frac{\rho RT}{M}\frac{(r-t_2)^2}{r_p^2}ln\left(\frac{P_2}{P_0}\right)$
F_6	$F_6 = \frac{A_p K_d}{\eta}\frac{P_1 - P_2}{l}$

used to calculate the total flow rate and water permeance. Besides the total flow rate and permeance as a function of temperature and pressure, the frequency of the flow modes is given as simulation output, to determine the predominant transport mechanism at each condition. The pore structure constant (K_d), the H_2O film thickness at the retentate and permeate side (i.e., t_1 and t_2, respectively) and the coefficient of resistance (C_r) could not be measured, so they were fitted comparing the model predictions against the permeability data from the permeation experiments using a least-square non-linear curve fitting algorithm (*lsqcurvefit*). Among these parameters, K_d and C_r are of particular interest since they both reflect the resistance to the flow exerted by the pore structure, which is believed to be influenced by the boehmite content.

Results and discussion

Characterization of the alumina phase in the Al-CMSM

The XRD patterns of the carbon films prepared with 0.8, 1.0 and 1.4 wt. % of boehmite are reported in Fig. 3a. The first and higher intensity peak appearing at 22° for the three samples is related to carbon [71]. Besides that, two main broad peaks appear for the 1.0 and 1.4 wt. % boehmite samples at 2θ value of 46° and 67°, which are related to the diffraction of the (440) and (400) planes of γ-Al_2O_3, respectively [72]. On the contrary, boehmite (γ-AlO(OH)) would have shown peaks centered at 48° and 65°, corresponding to the diffraction of the (200) and (002) planes. However, well dispersed and nanometer size boehmite sheets could not be detected. Indeed, at 0.8 wt% of boehmite, no peaks are observed between 30° and 90°, suggesting that the boehmite/γ-Al_2O_3 sheets are well dispersed in the carbon matrix, avoiding the crystallization. As the concentration of boehmite increases, clustering of the boehmite nano-sheets takes place, leading to their dehydration: 2 AlOOH ↔ γ-Al_2O_3 + H_2O [73]. As a result, at higher concentration of boehmite, the condensation of some of the nanosheets to the less hydrophilic γ-Al_2O_3 takes place, with no further phase-change towards the hydrophobic α-Al_2O_3. Fig. 3b displays the Al-region of the XPS pattern measured on the same carbon films. The deconvolution of the Al 2*p* peak shows the presence of both boehmite (AlO(OH)) and aluminum oxide (Al_2O_3), which is more pronounced for the 0.8 wt. % sample than for the more concentrated samples. Note that the exact amount of γ-Al_2O_3 and/or boehmite in the carbon layer after the carbonization is unknown, so these concentrations refer to the initial boehmite content in the dipping solution. Furthermore, analyzing the Al and C region, we confirm that the pyrolysis process did not cause any chemical interaction between them (see Fig. S3 in SI). The elemental composition of the carbon films was determined from the XPS spectra and the carbon to aluminum ratio is reported in Table 3.

Effect of alumina content on the Al-CMSMs hydrophilicity

Fig. 4 shows the effect of the initial boehmite content on the hydrophilicity of the carbon membranes studied by water adsorption experiments. The amount of water adsorbed increases with the boehmite content up to a maximum around 1 wt. %, showing then a decrease for the membranes with 1.2 and 1.4 wt. %. The membranes without any γ-Al_2O_3 already show a degree of hydrophilicity, as reported elsewhere [52,61] and confirmed by the water adsorbed by the 0 wt. % membrane (Fig. 4). When γ-Al_2O_3/γ- AlO(OH) nanosheets are integrated in the carbon matrix, it is clear that an optimum in concentration exists that maximizes the properties of the membrane (i.e., hydrophilicity). Moreover, at higher boehmite contents, the nanosheets of boehmite start to condensate (2 AlO(OH) ↔ γ-Al_2O_3 + H_2O) rendering a less hydrophilic cluster. The probability of condensation increases with the boehmite content. The presence of γ-Al_2O_3 is confirmed by the XRD (Fig. 3a).

Effect of the alumina content on the Al-CMSMs pore size distribution

The pore size distributions of the Al-CMSMs are reported in Fig. 5, covering the region of the micropores (i.e., $0.6 \leq d_p \leq 2$), which are more important for transport via adsorption-diffusion [53]. All the membranes show a very similar pore size distribution, with the most frequent size being around 1 nm. Therefore, we conclude that the alumina nanosheets do not affect the pore size distribution of the membranes in the pore size region covered by the N_2-permporometry technique (i.e. region of the micropores). However, we do not have information on the region of ultra-micropores (i.e., $d_p \leq 0.6$), which are responsible of the molecular sieving transport mechanism.

Effect of the alumina content on the thickness of the carbon layer

Fig. 6a and b shows a representative cross section of the Al-CMSMs prepared with 0.4 wt. % and 1.4 wt. % of boehmite, respectively, measured by SEM (see the other samples in SI). All the membranes were cut in different positions to confirm the uniformity of the layer thickness along the membrane. The average value of at least 3 measurements of the thickness of the composite layer is reported as a function of the initial boehmite content in Fig. 7. The Al-CMSMs show a clear

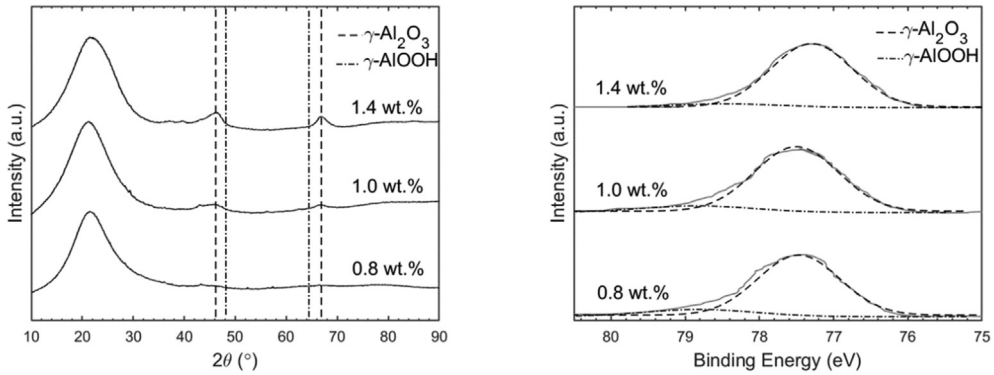

(a) (b)

Fig. 3 – XRD pattern (a) and Al-region of the XPS pattern (b) of the carbon films prepared from the dipping solution containing 0.8, 1.0 and 1.4 wt. % boehmite.

Table 3 – Carbon to aluminum ratio of the carbon films determined via the XPS analysis.

Init. Boehmite (wt.%)	C:Al (wt. based)
0.8	27.6
1.0	21.5
1.4	17.6

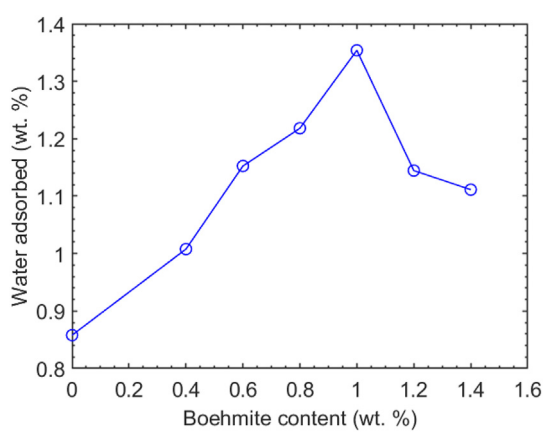

Fig. 4 – Amount of water adsorbed from the Al-CMSMs as a function of their boehmite content.

increase in the composite carbon-alumina layer thickness for larger alumina content, although the difference between CM12 and CM14 appear negligible. This is attributed to an increase of the viscosity of the dipping solution, which is a well-known parameter affecting the CMSM layer thickness [74]. Indeed, with higher boehmite concentration, the colloidal mixture becomes more viscous [75]. Note that other parameters that could affect the layer thickens (i.e., the dipping time, the porosity of the support) were kept constant.

Moreover, we believe that the sharper increase in the layer thickness at c.a. 1.2 wt. % of initial boehmite concentration is attributed to the rheological percolation of the dipping solution containing the boehmite nanosheets (i.e., concentration beyond which the bulk material shows a transition in physical properties, such as viscosity, in this case) [76].

Permeation results

The following section focuses on the results of the permeation experiments, first with pure vapor/gas to analyze the effect of the alumina content on the performance of all membranes, and later with binary mixtures, to understand the transport phenomena across a selected membrane.

All the membranes we tested in this study did not show any stability issue (i.e., permeance did not change significantly over time). Therefore, we conclude that no delamination phenomena occur and that the boehmite nanosheets did not affect the adherence of the carbon layer to the alumina support.

Effect of the alumina nanosheets on the Al-CMSMs permeation properties

In the field of inorganic membranes, the permeation is frequently reported as permeance (i.e., $\wp_i$ in mol m^{-2}s^{-1}Pa, defined as the permeated flux normalized by the driving force). However, in this study the water permeation is expressed in permeability (i.e., $\kappa_{H_2O} = \wp_{H_2O} \cdot l$, in mol m^{-1}s^{-1}Pa), to standardize the permeation properties with the membrane thickness, which increases with the boehmite content as discussed earlier (Fig. 7). Fig. 8 shows the water permeability (κ_{H_2O}) as a function of temperature and alumina content for the Al-CMSMs. Fig. 8a reveals that κ_{H_2O} monotonically decreases with temperature for all membranes, suggesting a strong contribution of capillary condensation and multi- and mono-layer adsorption diffusion as the main transport mechanisms [57]. Although the alumina content does not seem to influence the type of mechanism governing the water transport, it does show a clear effect on the permeability, as stressed in Fig. 8b. Regardless the operating temperature, we observe a volcano plot for κ_{H_2O} vs. initial boehmite loading, with a maximum in the κ_{H_2O} at 0.8 wt. % of initial boehmite content. This trend is, to some extent, consistent with the hydrophilicity trends reported in Fig. 4, except that they are peaked at slightly different with boehmite contents (i.e., 0.8 wt. % and 1 wt. %, respectively). This suggests a strong

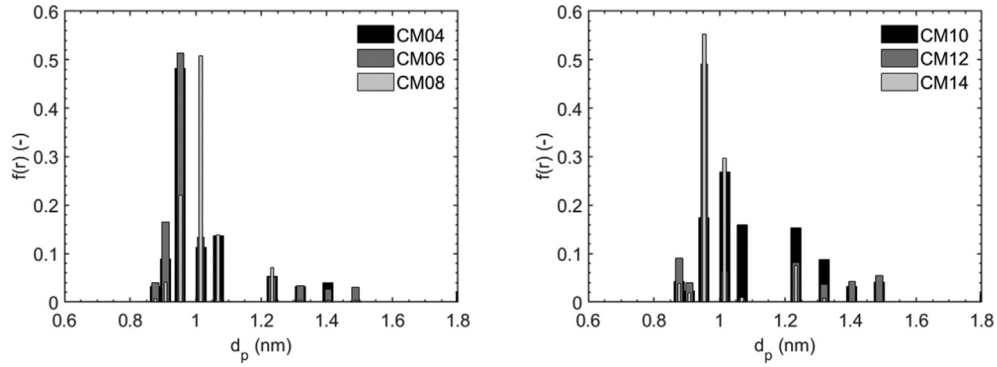

(a) (b)

Fig. 5 – Pore size distribution of the c-CMSMs with a boehmite content of 0.4 wt. %, 0.6 wt. % and 0.8 wt. % (a), and of 1.0 wt. %, 1.2 wt. % and 1.4 wt. % (b) derived with the permporometry technique.

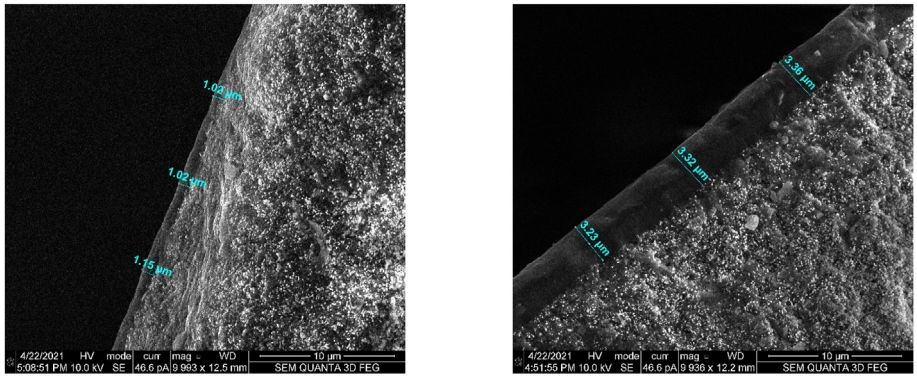

(a) (b)

Fig. 6 – Thickness of the carbon layer of the CM04 (a) and CM14 (b) measured on the images of the cross section of the membranes acquired with a FEI Quanta SEM.

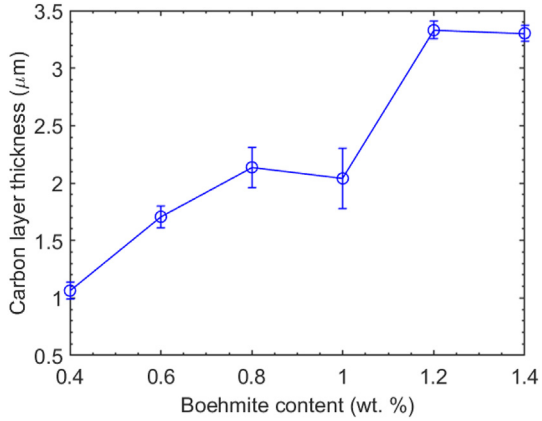

Fig. 7 – Average thickness of the composite carbon layer of the c-CMSM as a function of their initial boehmite content.

hydrophilicity-performance correlation, in line with the expectations for the transport via adsorption-diffusion. Nevertheless, the buildup in boehmite content from membrane CM08 to CM10, however, leads to a lower κ_{H_2O} despite the increase in the affinity to water. The higher hydrophilicity of these membranes increases the possibility of condensation of water, which render the transport in the pores slower. Note that the effects of layer thickness are normalized in the permeability data, and no major changes were found in the pore size distribution of these membranes, at least in the micropores region. Thus, we hypothesize that the introduction of alumina into the carbon structure induces certain changes into the porous structure of the selective layers (i.e., tortuosity and/or porosity), which may affect the transport of water, particularly at higher boehmite loadings. These effects will be further addressed in Section Effect of the alumina content on the thickness of the carbon layer.

Next, we extend our study to the permeation of other gases. Fig. 9a shows the permeability (logarithmic scale) as a function of the kinetic diameter of various gases at different temperatures of permeation. The permeability is the highest for the smallest gas (i.e., H_2O) and then it decreases when the kinetic diameter of the gas increases, which is clear indication of molecular sieving. However, N_2 shows the lowest permeability, being N_2 a molecule with very low polarizability and, as a consequence, not able to interact electrostatically with the hydrophilic pores. On the contrary, CO, despite being bigger that N_2, shows a higher permeability than N_2, due to its

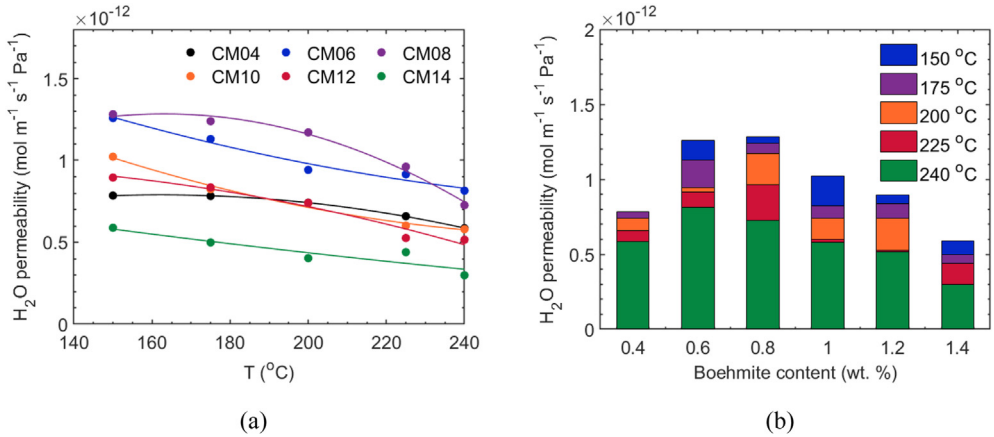

Fig. 8 – Water permeability as a function of the temperature of permeation for the Al-CMSMs prepared with different amount of boehmite (a) and as a function of the boehmite content at 150 °C, 200 °C, 225 °C and 240 °C (b). Other experimental conditions: $\Delta P = 3$ bar, 1 L·min^{-1} feed flow containing 7.5 vol% N_2.

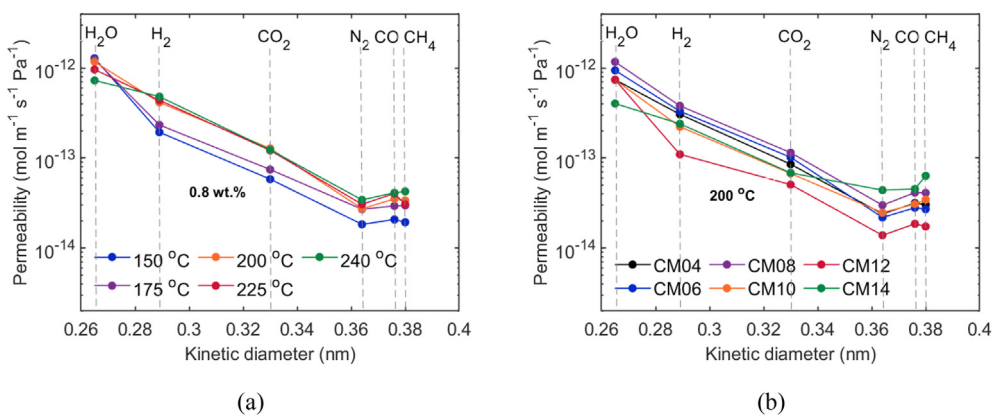

Fig. 9 – Permeability of each component (κ_i) as a function of their kinetic diameter, at various permeation temperatures for the membrane CM08 (a) and at 200 °C for the Al-CMSM containing different amount of boehmite (b).

polarity. For gases other than water, the permeability increases with the temperature. Similar results were obtained with the other membranes containing 0.4, 0.6, 1.0, 1.2 and 1.4% of boehmite in the dipping solution. Fig. 9b illustrates the permeability as a function of the kinetic diameter at 200 °C of the Al-CMSM with various content of boehmite. It can be observed that for most of the gases the permeability follows the order CM08> CM06> CM04> CM10 >CM14> CM12.

Fig. 10a, **b**, **c**, **d** and **e** report the ideal perm-selectivity as a function of temperature and of the boehmite content of the pairs H_2O/H_2, H_2O/CO_2, H_2O/N_2, H_2O/CO and H_2O/CH_4, respectively. The ideal perm-selectivity (H_2O/i) were determined by computing the ratio of the $\wp_{H_2O}$ and $\wp_i$ measured at the same temperature and pressure gradient, within the single gas/vapor permeation experiments. In line with the expectations, $S_{H_2O/i}$ generally increases for larger gas molecules, which is a clear indication of molecular sieving. However, the interactions between the permeating gases with the water adsorbed in the pores explain deviations with respect to the simple size-exclusion rationale. For example, the pair H_2O/N_2 shows the highest perm-selectivity (even higher than H_2O/CO and H_2O/CO_2) despite the fact that N_2 is not the largest molecule in this set, due to the lack of polarity. Yet, its relatively large size and low water solubility explain the high S_{H_2O/N_2}. On the other hand, the adsorption diffusion mechanism (i.e., direct gas adsorption on the pore walls) in the temperature range is not likely to occur for each of these gas, as reported in literature [44].

Fig. 10 also shows that all membranes exhibits a decreasing perm-selectivity with increasing temperature for each H_2O/i pair. As it is typical molecular sieving [77], the permeance of all the gases (reported in SI) shows a slight increase with temperature. Furthermore, when increasing the temperature, the water adsorbed in the pores will gradually desorb, driving to an increase in the active pore size [61,62,67]. However, even if $\wp_{H_2O}$ decreases with temperature, all the perm-selectivity assume values are >1 at each experimental condition, being water the most permeating species at all times.

Finally, the H_2O/i perm-selectivity generally increases with the initial boehmite content, which is largely explained by the decrease in permeance for all gases but water as the thickness (and likely the tortuosity/porosity, as previously hypothesized) of the composite carbon layer increases. With regards to water permeance, on the other hand, the boehmite content has a

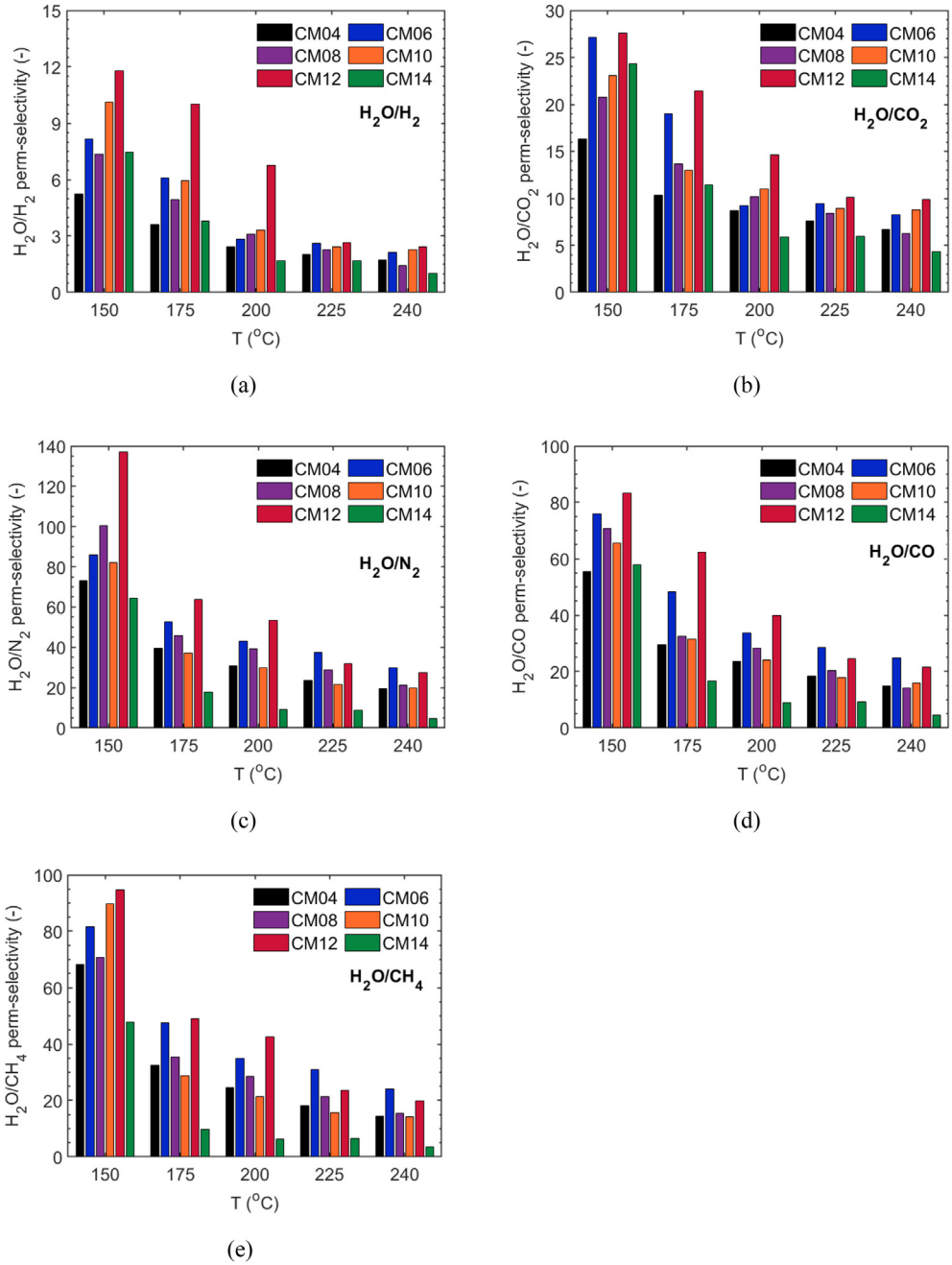

Fig. 10 – Ideal H_2O/H_2 (a) H_2O/CO_2 (b), H_2O/N_2 (c), H_2O/CO (d) and H_2O/CH_4 (e) perm-selectivity as a function of temperature for the Al-CMSMs prepared with different amount of boehmite. Other experimental conditions: $\Delta P = 3$ bar, 1 L·min^{-1} feed flow of gas. Ideal perm-selectivity were calculated as the ratio of $\wp_{H_2O}$ and $\wp_i$ measured at the same temperature and pressure gradient, within the single gas/vapor permeation experiments.

beneficial effect up to 0.8 wt. % due to the strengthening of the water-surface interactions derived from the higher number of hydrophilic sites, as previously established. Greater increase in boehmite loading also leads to lower water permeance, similar to all the other gases, but being water the smallest molecule as well as the most affine to the hydrophilic carbon surface, water permeation is less affected by any obstruction imposed by the structure of the carbon layer. It is also evident that the CM14 (i.e., the membrane with largest boehmite content) does not follow the above trend. It appears that the (limited) hydrophilicity of that sample (Fig. 4) does not provide sufficient water-surface interaction as compared to membranes with the slightly less boehmite, due to the condensation reaction of the molecules of AlO(OH). Thus, we conclude that the effect of the boehmite content on the hydrophilicity and on the membrane structure counterbalance each other, resulting again in a maximum in the perm-selectivity for the CM12 (i.e., 1.2 wt. % of boehmite).

Investigation on the permeation properties of the CM08 membrane

The selection of a membrane material for a specific process always rises from a trade-off between permeability and perm-selectivity [28]. From our previous work on CO_2 hydrogenation [22], given the membrane reactor configuration we propose (i.e., circulation of CO_2-H_2 sweep-gas), it was established that the most important parameter for this application is the $\wp_{H_2O}$, so the membrane we selected for a deeper investigation is the CM08.

First, we investigated the effect of the gradient in total pressure (ΔP) on the H_2O permeation and perm-selectivity toward H_2, CO_2 and CO (Fig. 11) at constant temperature (i.e., 150 °C). The $\wp_{H_2O}$ increases for larger ΔP, which confirms that the viscous flow of capillary condensate is indeed a main contributor to the transport mechanism. At the same time, $\wp_{H_2}$, $\wp_{CO_2}$ and $\wp_{CO}$ slightly decrease with ΔP (i.e., perm-selectivity increase with ΔP), leading again to the conclusion that the contribution of the adsorption diffusion is negligible in these conditions [78].

Secondly, we looked into the separation factors derived from the binary vapor/gas mixture tests (i.e., H_2O/H_2, H_2O/CO_2 and H_2O/CO real perm-selectivity), which are of interests for the reactions involving CO_2 and H_2 with the production of water. Fig. 12a, b, c show the effect of both temperature and gas/vapor composition in the feed on the separation factors of the pair H_2O/H_2 (SF_{H_2O/H_2}), H_2O/CO_2 (SF_{H_2O/CO_2}) and H_2O/CO ($SF_{H_2O/CO}$), respectively. The ideal perm-selectivity values are also reported as dashed line, for comparison. Generally, an increase in the gas composition (i.e., H_2, CO_2 or CO) causes a drop in the $SF_{H_2O/i}$ due to a lower driving force for the permeation of water (i.e., lower H_2O partial pressure gradient across the membrane). Furthermore, a lower separation factor can be interpreted as a result of the "competition" of H_2O and the second species for the hydrophilic sites in the pores. Among all, the SF_{H_2O/H_2} is the lowest, as expected considering the kinetic diameter of H_2O and H_2 (i.e., 0.26 and 0.29 nm, respectively). The interaction of a gas with water could be related with its solubility. However, given the constrictions of the pores, water behaves like a molecule rather than bulk water. As a result, it is even more correct to discuss about electrostatic interactions, which, anyway, follow the same trend as the solubility. Since H_2 shows a low solubility in water, especially at these conditions (i.e., lower than 0.001 g_{H_2}/kg_{H_2O}), and water has more affinity with the hydrophilic pores, water either blocks the pores completely where capillary condensation occurs (i.e., in the smallest pores) or it reduces the active pore size, where adsorption diffusion is predominant (i.e., in the slightly larger pores). Therefore, the real SF_{H_2O/H_2} is in general higher than the ideal H_2O/H_2 perm-selectivity, while it also decreases with temperature. On the contrary, the SF_{H_2O/CO_2} increases with temperature and is lower than the ideal perm-selectivity, particularly at low temperature. This clearly suggests that the high CO_2 solubility in water (ca. 0.5 g_{CO_2}/kg_{H_2O}) facilitates the permeation of CO_2 in the presence of water. As the CO_2 solubility in water (and thus the CO_2 permeation) decreases with temperature the SF_{H_2O/CO_2} increases. Lastly, the $SF_{H_2O/CO}$ is again lower than the ideal H_2O/CO perm-selectivity, especially at higher temperature. We ascribed this behaviour to the competitive adsorption between CO and water. Indeed, CO, due to its polarity, interacts more strongly with the pores of the membrane than all the other gases considered. In addition, the relatively large size of CO (i.e., 0.376 nm, similar to the size of ultra-micropores) can also cause pore clogging, hindering permeance of water.

Modelling results

In this section, we discuss the results obtained with the *6 flows model*. The routine we implemented in MATLAB allowed us to identify the flow mode at each pore size, by imposing the boundary conditions at the upstream and downstream side of the membrane pores (i.e., retentate and permeate) according to the experimental conditions. Therefore, we believe that the transport mechanisms of pure water through the pores and their relative occurrence are fully representative of the phenomena occurring at the pore scale. However, parameter fitting on the permeability data was required to derive properties of the complex porous structure of the carbon layer that could not be determined experimentally. First, we focus on the water transport phenomena by fitting the experimental data from the best performing membrane CM08. Fig. 13a shows the result of the curve fitting of the $\wp_{H_2O}$ as a function

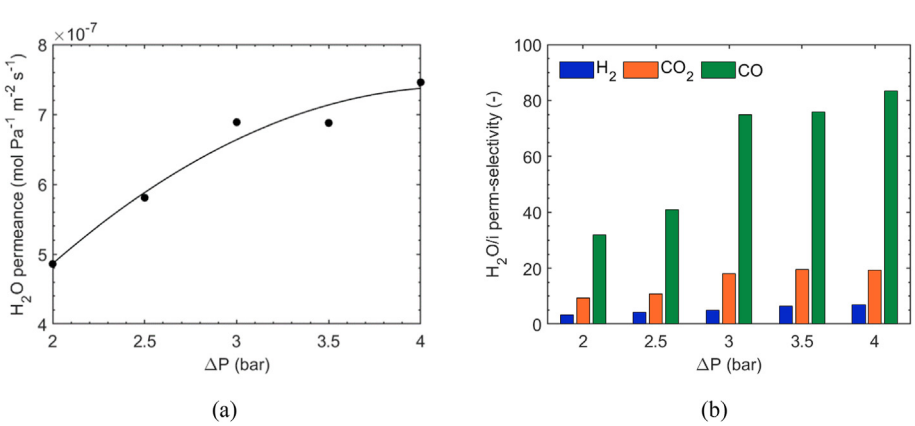

Fig. 11 – Water permeance (a) and ideal H_2O/i perm-selectivity (b) as a function of the gradient in total pressure measured at 150 °C for the CM08 membrane.

Please cite this article as: Poto S et al., Vapor/gas separation through carbon molecular sieve membranes: Experimental and theoretical investigation, International Journal of Hydrogen Energy, https://doi.org/10.1016/j.ijhydene.2021.10.155

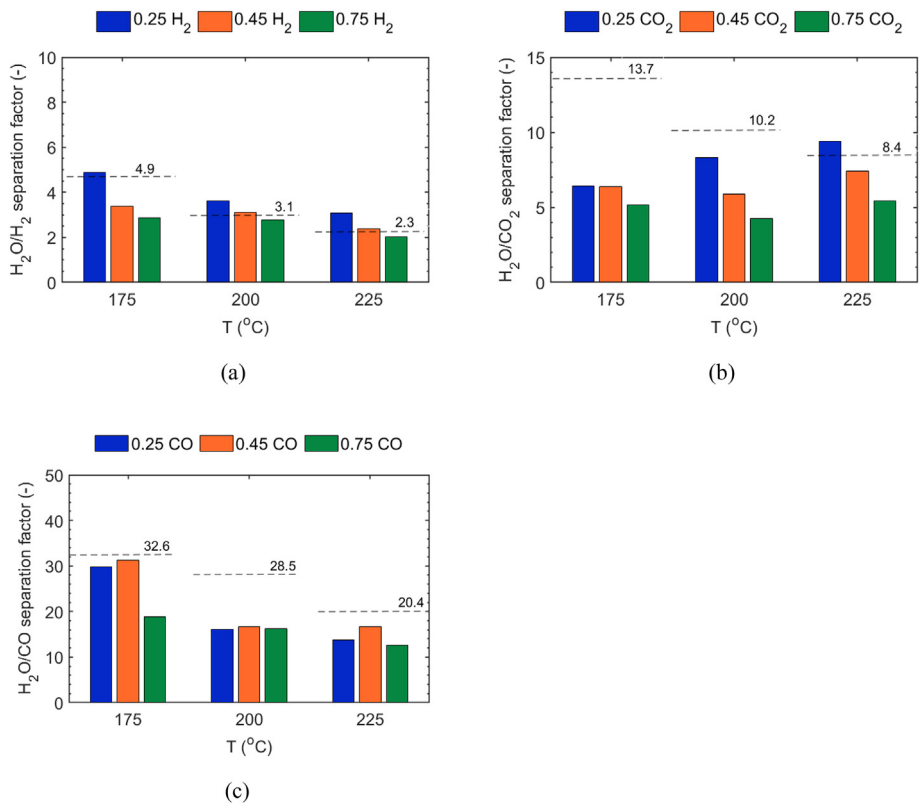

Fig. 12 – Separation factors of: a) the pair H_2O/H_2 (SF_{H_2O/H_2}), b) H_2O/CO_2 (SF_{H_2O/CO_2}) and c) H_2O/CO ($SF_{H_2O/CO}$) as a function of temperature and feed composition. The gradient in total pressure was set at 3 bar and the total flow through the membrane was 1 L·min^{-1}. A 10% of N_2 was always included in the feed, to ensure the correct functioning of the C.E.M. Dashed lines indicate the ideal perm-selectivity of each H_2O/gas pair, measured at the same temperature.

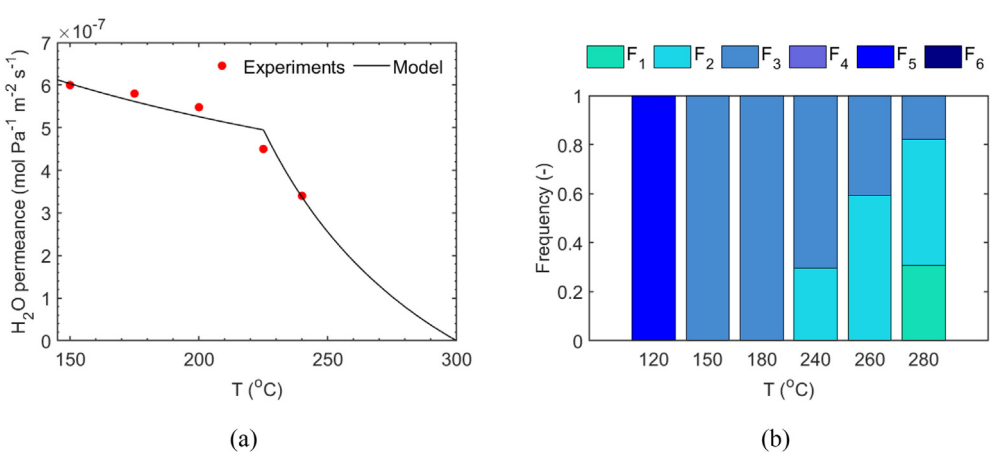

Fig. 13 – Comparison of the modelling and experimental results of the $\wp_{H_2O}$ as a function of temperature of the CM08 membrane (a). The experimental results reported in Fig. 8 (red circles) were fitted with the 6 flows model (continuous black line). The frequency of occurrence of each flow mode as a function of temperature is also reported (b). (For interpretation of the references to colour in this figure legend, the reader is referred to the Web version of this article.)

of temperature (i.e., data reported in Fig. 8). At 225 °C the curve shows a discontinuity which is ascribed to the evaporation of part of the capillary condensate at the downstream side (i.e., F_2 contribution starts to be relevant). The picture is even clearer when looking at the frequency of each type of flow as a function of temperature (Fig. 13b). In the lowest temperature range considered (i.e., 120 °C), the entire pore is filled with a capillary condensate and the upstream end of the pore is filled with bulk condensate. (i.e., F_5). As temperature increases from 120 °C to 180 °C, both pore ends are in contact with the bulk

vapor phase (i.e., there is no bulk phase condensation of water at these conditions), while the entire pore remains filled with capillary condensate (i.e., F_3). In this case, the viscous flow of the capillary condensate is the dominant transport mechanism. Further increase in temperature above 180 °C shows a gradual transition to F_2, where capillary condensation only occurs at the upstream end of the pore, while the downstream end contains gas and water adsorbate. Further, we predict that for temperature higher than 260 °C, the multi-layer adsorption diffusion (F_1) starts to contribute more significantly, although experimental validation beyond 240 °C is still required. The flow modes F_4 and F_6 do not show any contribution in the conditions explored experimentally (i.e., the conditions defining F_4 and F_6 reported in Fig. 2 do not occur). However, predictions beyond the range of the experimental conditions should be validated experimentally. In particular, the model becomes less accurate in predicting the transition to a different type of flow.

Next, we assess the effect of pressure gradient across the membrane (ΔP) with the same model. To that end, the $\wp_{H_2O}$ data derived at different ΔP at 150 °C were simulated (Fig. 14). According to our experiments, no significant changes in the transport mechanism of water is observed in the range of pressure gradients explored in this study (i.e., F_5 is the dominant flow mode). Nevertheless, the model predicts a change in the flow mode when increasing the ΔP beyond 3.8 bar, which is very close to our last experimental point. According to this prediction, the $\wp_{H_2O}$ is expected to reach an asymptotic value, which unfortunately could not be validated experimentally due to the limitations of the experimental setup.

Finally, the $\wp_{H_2O}$ data as a function of temperature of all the membranes were fitted in the range 150–220 °C, where a semi-linear behaviour of $\wp_{H_2O}$ was identified (details in SI). An interesting outcome of this curve fitting is the value of K_d,

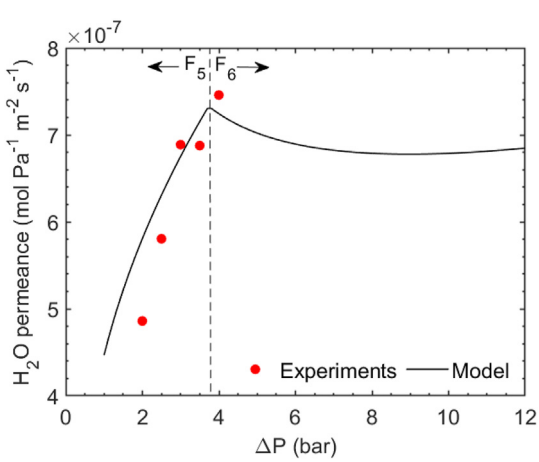

Fig. 14 – Comparison of the modelling and experimental results of the $\wp_{H_2O}$ as a function of pressure of the CM08 membrane. The experimental results reported in Fig. 10 (red circles) were fitted with the 6 flows model (continuous black line). The dominant flow mode is reported in the same figure: flow mode F_5 converge into flow mode F_6 at 3.8 bar (dashed line). (For interpretation of the references to colour in this figure legend, the reader is referred to the Web version of this article.)

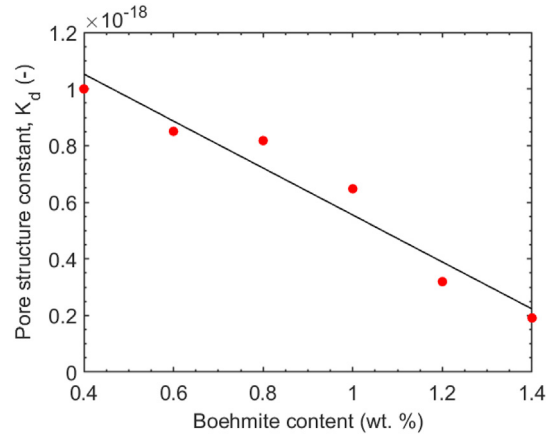

Fig. 15 – Pore structure constant (K_d) derived from the parameter fitting as a function of the boehmite content. Discrete values (red circles) were fitted with a linear regression (black line). (For interpretation of the references to colour in this figure legend, the reader is referred to the Web version of this article.)

which is a geometrical factor that describes the structure of the porous system (i.e., larger K_d values represent a lower resistance to the transport). In particular, $K_d$plays a role in the flow mode F_3 (see Table 2), which is the dominant mechanism in wide range of experimental conditions studied in this work. Fig. 15 shows the K_d values of all membranes tested, showing a linear inverse correlation with the boehmite content of the carbon membranes. This result support our earlier hypothesis that the boehmite/alumina sheets alter the structure of the porous system, generally hindering the permeation of most of the species as the alumina content increases. Oftentimes this is explained by the formation of defects, which are zones where the permeation decreases because the species are forced to increase the path length (i.e., increase in tortuosity). This finding supports both the decrease in the permeability of the membranes prepared with higher boehmite content and the optimum found in the water permeability and perm-selectivity.

Conclusions

In this work, several boehmite-phenolic resin composite carbon molecular sieve membranes were prepared by the one dip-dry-carbonization step method, using different boehmite content in the dipping solution (ranging from 0.4 to 1.4 wt. %). The membranes were tested in view of their application for the water-vapor separation in membrane reactors. The hydrophilic boehmite nanosheets were used as precursor of γ-Al_2O_3 to increase the adsorption of water and increase its transport mechanism by diffusion. We observed that the alumina content increases the hydrophilicity of the Al-CMSM up to an optimum at c.a. 1.0 wt. %. At larger boehmite content the affinity to water decreases because: 1) the probability of boehmite condensation to the less hydrophilic γ-Al_2O_3 is higher and 2) the C:Al ratio corresponding to c.a. 1.0 wt% of boehmite content maximizes the membrane

Please cite this article as: Poto S et al., Vapor/gas separation through carbon molecular sieve membranes: Experimental and theoretical investigation, International Journal of Hydrogen Energy, https://doi.org/10.1016/j.ijhydene.2021.10.155

properties. The alumina content does not significantly affect the pore size distribution of the membranes, at least in the region of micropores. On the other hand, the cross section of the Al-CMSMs show an increase in the thickness of the composite carbon layer for larger alumina content. We noticed that the water permeability shows an optimum with the initial boehmite content around 0.8 wt%, which is in line with the increase in hydrophilicity of the membranes. For higher alumina content, the $\kappa_{H_2O}(T)$ decreases. This decrease is induced both by a lower hydrophilicity and by a difference in the structure of the porous system (i.e., tortuosity and/or porosity), introduced by the boehmite/alumina sheets. Similarly, the ideal perm-selectivity of H_2O towards H_2, CO_2, CO, N_2 and CH_4 increases with the alumina content, showing an optimum with the C:Al ratio (i.e., initial boehmite content of 1.2 wt %). Among all the membranes tested in this study, the CM08 (i.e., membrane prepared with initial boehmite content of 0.8 wt%), show the best combination of H_2O permeability and perm-selectivity. A further investigation on the permeation properties of this membranes revealed that the H_2O/gas interaction plays an important role in the vapor/gas separation. In particular, the CO_2 electrostatic interaction with water causes lower separation factors when measured from feed containing both H_2O and CO_2 (i.e., real separation factor). On the contrary, the SF_{H_2O/H_2} shows higher values with respect to the corresponding ideal perm-selectivity, due to the pore-blocking effect derived from the water capillary condensation in the pores. Lastly, the $SF_{H_2O/CO}$ displays values lower than the ideal H_2O/CO perm-selectivity, especially at higher temperature. This behaviour was ascribed to the possibility of CO to clog some of the pores where water has not yet adsorbed or condensed. In general, we found that the $\wp_{H_2O}$ and H_2O/i selectivity decrease with temperature and increase with ΔP. The 6 *flows model* indicates that the water vapor flow through the carbon pores transforms from capillary condensation to multi- and monolayer surface flow combined with molecular Knudsen gas flow, as temperature increases. When increasing the applied pressure difference at 150 °C, the water vapor permeance becomes higher, indicating the role of capillary condensation. However, the model predicts an asymptotic behaviour for ΔP of approximately 3.8 bar.

In conclusion, this work shows that the composite alumina supported CMSM are promising material for the water separation from gaseous mixtures at relatively high temperatures (i.e., 150–250 °C), conditions which are compatible with the CO_2 conversion to methanol and/or DME reactions. Their separation performance, combined with the high stability of these materials, make these membrane very good candidates for their use in membrane reactors where the in *in-situ* removal of water is required.

Declaration of competing interest

The authors declare that they have no known competing financial interests or personal relationships that could have appeared to influence the work reported in this paper.

Acknowledgements

This project has received funding from the European Union's Horizon 2020 research and innovation programme under grant agreement No 838014 (*C2Fuel* project).

Appendix A. Supplementary data

Supplementary data to this article can be found online at https://doi.org/10.1016/j.ijhydene.2021.10.155.

REFERENCES

[1] Shuit Siew Hoong, et al. Membrane technology as a promising alternative in biodiesel production: a review. Biotechnol Adv 2012;30(6):1364–80.
[2] He Rongjie, et al. A mid/low-temperature solar-driven integrated membrane reactor for the dehydrogenation of propane–A thermodynamic assessment. Appl Therm Eng 2021;193:116952.
[3] Walter Jan P, et al. Model-based analysis of fixed-bed and membrane reactors of various scale. Chem Ing Tech 2021;93(5):819–24.
[4] Shuit, Siew Hoong, et al. Membrane technology as a promising alternative in biodiesel production: a review. Biotechnol Adv 2012;30(6):1364–80.
[5] Dijkstra Jan Wilco, et al. Development of membrane reactor technology for power production with pre-combustion CO2 capture. Energy Procedia 2011;4:715–22.
[6] Gallucci Fausto. Inorganic Membrane reactors for methanol synthesis. In: Methanol. Elsevier; 2018. p. 493–518.
[7] Espinoza RL, et al. Use of membranes in Fischer-Tropsch reactors. In: Studies in surface science and catalysis, vol. 130. Elsevier; 2000. p. 389–94.
[8] Leonzio Grazia, Zondervan Edwin, Foscolo Pier Ugo. Methanol production by CO2 hydrogenation: analysis and simulation of reactor performance. Int J Hydrogen Energy 2019;44(16):7915–33.
[9] Atsonios Konstantinos, Panopoulos Kyriakos D, Kakaras Emmanuel. Investigation of technical and economic aspects for methanol production through CO2 hydrogenation. Int J Hydrogen Energy 2016;41(4):2202–14.
[10] Lim Rern Jern, et al. A review on the electrochemical reduction of CO2 in fuel cells, metal electrodes and molecular catalysts. Catal Today 2014;233:169–80.
[11] Iaquaniello G, et al. CO2 valorization through direct methanation of flue gas and renewable hydrogen: a technical and economic assessment. Int J Hydrogen Energy 2018;43(36):17069–81.
[12] Atsbha, Aregawi Tesfalem, et al. A review on the catalytic conversion of CO2 using H2 for synthesis of CO, methanol, and hydrocarbons. J CO2 Util 2021;44:101413.
[13] Roy Soumyabrata, Cherevotan Arjun, Peter Sebastian C. Thermochemical CO2 hydrogenation to single carbon products: scientific and technological challenges. ACS Energy Lett 2018;3(8):1938–66.
[14] Prieto Gonzalo. Carbon dioxide hydrogenation into higher hydrocarbons and oxygenates: thermodynamic and kinetic bounds and progress with heterogeneous and homogeneous catalysis. ChemSusChem 2017;10(6):1056–70.

[15] Iliuta I, Larachi F, Fongarland P. Dimethyl ether synthesis with in situ H2O removal in fixed-bed membrane reactor: model and simulations. Ind Eng Chem Res 2010;49(15):6870–7.
[16] Diban Nazely, et al. Improved performance of a PBM reactor for simultaneous CO2 capture and DME synthesis. Ind Eng Chem Res 2014;53(50):19479–87.
[17] De Falco, Marcello Mauro Capocelli, Basile Angelo. Selective membrane application for the industrial one-step DME production process fed by CO2 rich streams: modeling and simulation. Int J Hydrogen Energy 2017;42(10):6771–86.
[18] Diban Nazely, et al. Influence of the membrane properties on the catalytic production of dimethyl ether with in situ water removal for the successful capture of CO2. Chem Eng J 2013;234:140–8.
[19] Farsi M, Hallaji Sani A, Riasatian P. Modeling and operability of DME production from syngas in a dual membrane reactor. Chem Eng Res Des 2016;112:190–8.
[20] Rodriguez-Vega Pablo, et al. Experimental implementation of a catalytic membrane reactor for the direct synthesis of DME from H2+ CO/CO2. Chem Eng Sci 2021;234:116396.
[21] Ateka Ainara, et al. Strategies for the intensification of CO2 valorization in the one-step dimethyl ether synthesis process. Ind Eng Chem Res 2019;59(2):713–22.
[22] Poto S, Gallucci F, Neira MF. Direct conversion of CO 2 to dimethyl ether in a fixed bed membrane reactor : influence of membrane properties and process conditions. Fuel 2021;302(February):121080.
[23] Salehi Mohammad-Sadegh, et al. Selective CO2-Hydrogenation using a membrane reactor. Chem Eng Process 2021;160:108264.
[24] Gallucci Fausto, Basile Angelo. A theoretical analysis of methanol synthesis from CO2 and H2 in a ceramic membrane reactor. Int J Hydrogen Energy 2007;32(18):5050–8.
[25] Lee Kew-Ho, Youn Min-Young, Sea Bongkuk. Preparation of hydrophilic ceramic membranes for a dehydration membrane reactor. Desalination 2006;191(1–3):296–302.
[26] Piera Elena, et al. Synthesis, characterization and separation properties of a composite mordenite/ZSM-5/chabazite hydrophilic membrane. J Membr Sci 1998;149(1):99–114.
[27] Raso R, et al. Zeolite membranes: comparison in the separation of H2O/H2/CO2 mixtures and test of a reactor for CO2 hydrogenation to methanol. Catal Today 2021;364:270–5.
[28] Rohde MP, et al. Fischer–Tropsch synthesis with in situ H2O removal–directions of membrane development. Microporous Mesoporous Mater 2008;115(1–2):123–36.
[29] Sommer Stefan, Melin Thomas. Influence of operation parameters on the separation of mixtures by pervaporation and vapor permeation with inorganic membranes. Part 1: dehydration of solvents. Chem Eng Sci 2005;60(16):4509–23.
[30] Qiao Zhihua, et al. PVAm–PIP/PS composite membrane with high performance for CO 2/N 2 separation. AIChE J 2013;59(1):215–28.
[31] Gallucci Fausto, Paturzo Luca, Basile Angelo. An experimental study of CO2 hydrogenation into methanol involving a zeolite membrane reactor. Chem Eng Process: Process Intensification 2004;43(8):1029–36.
[32] Rohde Martin P, Unruh Dominik, Schaub Georg. Membrane application in Fischer– Tropsch synthesis to enhance CO2 hydrogenation. Ind Eng Chem Res 2005;44(25):9653–8.
[33] Hedlund Jonas, et al. A masking technique for high quality MFI membranes. J Membr Sci 2003;222(1–2):163–79.
[34] Lai Re, Gavalas George R. Surface seeding in ZSM-5 membrane preparation. Ind Eng Chem Res 1998;37(11):4275–83.
[35] Ravenelle Ryan M, et al. Stability of zeolites in hot liquid water. J Phys Chem C 2010;114(46):19582–95.
[36] Ismail Ahmad Fauzi, David LIB. Future direction of R&D in carbon membranes for gas separation. Membr Technol 2003;4(2003):4–8.
[37] Rodrigues Sandra C, et al. Carbon membranes with extremely high separation factors and stability. Energy Technol 2019;7(4):1801089.
[38] Ismail Ahmad Fauzi, David LIB. A review on the latest development of carbon membranes for gas separation. J Membr Sci 2001;193(1):1–18.
[39] Pontzen Florian, et al. CO2-based methanol and DME–efficient technologies for industrial scale production. Catal Today 2011;171(1):242–50.
[40] Götz Manuel, McDaniel Koch Amy, Graf Frank. State of the art and perspectives of CO2 methanation process concepts for power-to-gas applications. In: International gas union research conference, vol. 13. Fornebu, Norway: International Gas Union; 2014.
[41] Saufi SM, Ismail AF. Fabrication of carbon membranes for gas separation––a review. Carbon 2004;42(2):241–59.
[42] He Xuezhong, et al. CO2 capture by hollow fibre carbon membranes: experiments and process simulations. Energy Procedia 2009;1(1):261–8.
[43] Fuertes Antonio B, Menendez Ivan. Separation of hydrocarbon gas mixtures using phenolic resin-based carbon membranes. Separ Purif Technol 2002;28(1):29–41.
[44] Tanco Margot A Llosa, et al. Hydrogen permeation studies of composite supported alumina-carbon molecular sieves membranes: separation of diluted hydrogen from mixtures with methane. Int J Hydrogen Energy 2021;46(37):19758–67.
[45] Rao MadhukarB, Sircar Shivaji. Nanoporous carbon membranes for separation of gas mixtures by selective surface flow. J Membr Sci 1993;85(3):253–64.
[46] Briceño Kelly, et al. Carbon molecular sieve membranes supported on non-modified ceramic tubes for hydrogen separation in membrane reactors. Int J Hydrogen Energy 2012;37(18):13536–44.
[47] He Xuezhong. Techno-economic feasibility analysis on carbon membranes for hydrogen purification. Separ Purif Technol 2017;186:117–24.
[48] Wang Qixiang, et al. Carbon molecular sieve membranes derived from crosslinkable polyimides for CO2/CH4 and C2H4/C2H6 separations. J Membr Sci 2021;621:118785.
[49] Lei L, Lindbråthen A, Hillestad M, He X. Carbon molecular sieve membranes for hydrogen purification from a steam methane reforming process. J Membr Sci 2021;627(March):119241. https://doi.org/10.1016/j.memsci.2021.119241.
[50] Tanihara Nozomu, et al. Gas permeation properties of asymmetric carbon hollow fiber membranes prepared from asymmetric polyimide hollow fiber. J Membr Sci 1999;160(2):179–86.
[51] Fuertes Antonio B. Adsorption-selective carbon membrane for gas separation. J Membr Sci 2000;177(1–2):9–16.
[52] Forster Luke, et al. Tailoring pore structure and surface chemistry of microporous Alumina-Carbon Molecular Sieve Membranes (Al-CMSMs) by altering carbonization temperature for optimal gas separation performance: an investigation using low-field NMR relaxation measurements. Chem Eng J 2021:129313.
[53] Hamm Janice BS, et al. Recent advances in the development of supported carbon membranes for gas separation. Int J Hydrogen Energy 2017;42(39):24830–45.
[54] Kiyono Mayumi, Williams Paul J, Koros William J. Effect of pyrolysis atmosphere on separation performance of carbon molecular sieve membranes. J Membr Sci 2010;359(1–2):2–10.

Please cite this article as: Poto S et al., Vapor/gas separation through carbon molecular sieve membranes: Experimental and theoretical investigation, International Journal of Hydrogen Energy, https://doi.org/10.1016/j.ijhydene.2021.10.155

[55] Gilron J, Soffer A. Knudsen diffusion in microporous carbon membranes with molecular sieving character. J Membr Sci 2002;209(2):339–52.
[56] Ismail Ahmad Fauzi, et al. Transport mechanism of carbon membranes. In: Carbon-based membranes for separation processes. New York, NY: Springer; 2011. p. 5–16.
[57] Uhlhorn RJR, Keizer Klaas, Burggraaf AJ. Gas transport and separation with ceramic membranes. Part I. Multilayer diffusion and capillary condensation. J Membr Sci 1992;66(2–3):259–69.
[58] Lee Kew-Ho, Hwang Sun-Tak. The transport of condensible vapors through a microporous Vycor glass membrane. J Colloid Interface Sci 1986;110(2):544–55.
[59] Horikawa Toshihide, Do DD, Nicholson D. Capillary condensation of adsorbates in porous materials. Adv Colloid Interface Sci 2011;169(1):40–58.
[60] Fisher LR, Israelachvili JN. Direct experimental verification of the Kelvin equation for capillary condensation. Nature 1979;277(5697):548–9.
[61] Jones Cheryl W, Koros William J. Characterization of ultramicroporous carbon membranes with humidified feeds. Ind Eng Chem Res 1995;34(1):158–63.
[62] Lagorsse S, Magalhães FD, Mendes A. Aging study of carbon molecular sieve membranes. J Membr Sci 2008;310(1–2):494–502.
[63] Tseng Hui-Hsin, Shiu Pei-Ting, Lin Yi-Shan. Effect of mesoporous silica modification on the structure of hybrid carbon membrane for hydrogen separation. Int J Hydrogen Energy 2011;36(23):15352–63.
[64] Teixeira Miguel, et al. Boehmite-phenolic resin carbon molecular sieve membranes—permeation and adsorption studies. Chem Eng Res Des 2014;92(11):2668–80.
[65] Tanco Margot A Llosa, et al. Composite-alumina-carbon molecular sieve membranes prepared from novolac resin and boehmite. Part I: preparation, characterization and gas permeation studies. Int J Hydrogen Energy 2015;40(16):5653–63.
[66] Tanco Margot A Llosa, Pacheco Tanaka David A, Mendes Adélio. Composite-alumina-carbon molecular sieve membranes prepared from novolac resin and boehmite. Part II: effect of the carbonization temperature on the gas permeation properties. Int J Hydrogen Energy 2015;40(8):3485–96.
[67] Jones Cheryl W, Koros William J. Carbon composite membranes: a solution to adverse humidity effects. Ind Eng Chem Res 1995;34(1):164–7.
[68] Tsuru Toshinori, et al. Permporometry characterization of microporous ceramic membranes. J Membr Sci 2001;186(2):257–65.
[69] Uhlhorn RJR, Keizer Klaas, Burggraaf AJ. Gas transport and separation with ceramic membranes. Part I. Multilayer diffusion and capillary condensation. J Membr Sci 1992;66(2–3):259–69.
[70] Rhim Hannong, Hwang Sun-Tak. Transport of capillary condensate. J Colloid Interface Sci 1975;52(1):174–81.
[71] López-Romero S, Chávez-Ramírez J. Synthesis of TiC thin films by CVD from toluene and titanium tetrachloride with nickel as catalyst. Materia 2007;12(3):487–93.
[72] Zhang Xiaoxue, et al. Transition alumina nanoparticles and nanorods from boehmite nanoflakes. J Cryst Growth 2008;310(15):3674–9.
[73] Paglia Gianluca, et al. Boehmite derived γ-alumina system. 1. Structural evolution with temperature, with the identification and structural determination of a new transition phase, γ '-alumina. Chem Mater 2004;16(2):220–36.
[74] Strawbridge I, James PF. The factors affecting the thickness of sol-gel derived silica coatings prepared by dipping. J Non-Cryst Solids 1986;86(3):381–93.
[75] Senapati PK, Mishra BK, Parida A. Modeling of viscosity for power plant ash slurry at higher concentrations: effect of solids volume fraction, particle size and hydrodynamic interactions. Powder Technol 2010;197(1–2):1–8.
[76] Abraham Jiji, et al. Rheological percolation in thermoplastic polymer nanocomposites. J Rheol 2017;1:1–15.
[77] Medrano JA, et al. Transport mechanism and modeling of microporous carbon membranes. In: Current trends and future developments on (bio-) membranes. Elsevier; 2019. p. 39–58.
[78] Koresh Jacob E, Abraham Soffer. Mechanism of permeation through molecular-sieve carbon membrane. Part 1.—the effect of adsorption and the dependence on pressure. J Chem Soc, Faraday Trans 1: Physical Chemistry in Condensed Phases 1986;82(7):2057–63.

Please cite this article as: Poto S et al., Vapor/gas separation through carbon molecular sieve membranes: Experimental and theoretical investigation, International Journal of Hydrogen Energy, https://doi.org/10.1016/j.ijhydene.2021.10.155